Materials Transactions, JIM, Vol. 37, No. 4 (1996), pp. 627 to 635

Synthesis and Formation Mechanism of Ultrafine Spherical Al_2O_3 Powders by Ultrasonic Spray Pyrolysis

V. Jokanović*, Dj. Janaćković**, A. M. Spasić* and D. Uskoković***

*Institute for Technology of Nuclear and Other Mineral Row Materials, Belgrade, Yugoslavia
**Faculty of Technology and Metallurgy, University of Belgrade, Yugoslavia
***Institute of Technical Sciences of the Serbian Academy of Sciences and Arts, Belgrade, Yugoslavia

Synthesis of high-purity submicrometer spherical particles of α-alumina is performed by ultrasonic spray pyrolysis. As precursors, 0.5 M water solutions of both $AlCl_3 \cdot 6H_2O$ and $Al(NO_3)_3 \cdot 9H_2O$ have been used. The influence of aerosol droplet genesis on the particle size distribution of α-alumina is regarded as a main control parameter. In the case of very fine droplets (smaller than 0.3 μm), regardless of the precursor, the precipitation of dissolved compound inside the droplet occurs by the volume precipitation mechanism. Morphology of the particles corresponds to that of the realized aerosol droplets. An increased activity of produced powders enables the phase transformation of γ- to α-alumina in the temperature range 1073 ~ 1173 K, while at 1273 K the transformation process is complete.

(Received July 14, 1995)

Keywords: *ultrasonic spray pyrolysis, spherical Al_2O_3 powders, ultrafine particle morphology, synthesis, phase transformation, particle size distribution*

I. Introduction

For successful applications in electronics, Al_2O_3 ceramics ought to have low dielectric constant, high specific resistance, thermal and chemical stability, high heat conductivity, and low surface roughness. Such properties make this ceramic material useful for the fabrication of components, for electronic tube housings, metalloceramic seals in high vacuum equipments, as well as for the substrates of multi-layer tightly packed integrated circuits (modules), tube transmitters. For some other applications, *e.g.* in medicine, mechanical and aerospace engineering, mechanical (static and dynamic) properties are very important. For these purposes, the synthesized material ought to be very pure and have an ideal density and perfectly uniform microstructure with small grains.

To fulfil such requirements, many different processes of alumina synthesis have been developed such as: direct oxidation of the metal in H_2/O_2 flame (flame reaction), oxidation of fine metal powders by water vapour in an autoclave, pyrolytic decomposition of organic and inorganic compounds, sol-gel process, spray pyrolysis using a twin-fluid atomizer, nebulizer or an ultrasonic atomizer, conventional chemical vapour deposition (CVD) or assisted by different types of plasma processes, etc.[1)-7)].

The production of fine ceramic powders by spray pyrolysis, using an ultrasonic atomizer, enables design of spherical particle diameters, as the basic element of the system, and consequently, the programmed synthesis of the material by suitable consolidation technique.

Depending on the properties of precursors and process parameters, it is possible to obtain powders with different characteristics, packing densities and distribution of structure elements inside the particles, important for the behaviour of the system during consolidation.

An industrial method for the synthesis of very pure α-alumina by spray pyrolysis using $AlCl_3 \cdot 6H_2O$ as a precursor has been firstly developed by Ruthner and Krischner[8]. As shown, the phase transformations depend on the heating rate. At low heating rates γ-Al_2O_3 formed and then α-Al_2O_3 at 1173 K. At rapid heating rates α-Al_2O_3 directly formed from the amorphous phase.

Dornier company[9] has developed an industrial method for alumina powder synthesis by the spray pyrolysis. For the production of Al_2O_3–ZrO_2 reinforced ceramics, different organic and inorganic salts of Al, Zr, and Y (chlorides, nitrates, and acetates) have been used as precursors. Sinterability of the produced powder is high, and sintered samples have, practically, theoretical densities and good mechanical characteristics.

Roy *et al.*[10] have investigated alumina formation from the precursor $Al(NO_3)_3 \cdot 9H_2O$. Amorphous Al_2O_3 has been formed in the temperature range 1173 ~ 1193 K. After 1 h heating at 1173 K, α-Al_2O_3 has been obtained. As found, the degree of crystallinity significantly depends not only on temperature but on the length of heating zone as well, i.e. on the particle residence time inside the reactor. It has been also found that the concentration of initial solution and the atomization pressure influence the particle size.

Zhang and Messing[11] have investigated the influence of temperature coefficient of salts solubility on the formation of Al_2O_3 particles. From $Al_2(SO_4)_3$, which has a positive temperature coefficient of solubility, the non-porous spherical particles of 0.5 ~ 1.5 μm diameters have been

obtained. However, if the alumina particles are produced from $Al(NO_3)_3 \cdot 9H_2O$, then the particles with "foam" structure will be obtained, as a result of Al-nitrate melting at 349 K, and because of the removal of nitrate gases[12]. Below the nitrate melting point, NH_3 is to be inserted to enable the precipitation by the volume mechanism. It results in the hydrolysis and the precipitation in the bulk of droplets.

Previous investigations have shown that the mechanism of particle precipitation during the spray pyrolysis depends on the following: the type of precursor, conditions of atomization, concentration of salt solution, physical and chemical properties of salts, precipitation temperature (the coefficient of thermal solubility of salts), percolation index, difference between the temperatures of critical supersaturation and of equilibrium saturation of the precipitating system, ratio of the solution diffusion coefficient to the heat conductivity of the system, rate of solvent evaporation, rate of drying, and the properties of particle surfaces (*e.g.* the permeability). Depending on the various parameters, it is possible to produce particles by volume or by surface precipitation. It has been already shown that the choice of precursor has the most important influence on the mechanism of particles precipitation and on the particle behaviour during consolidation. In the case of very fine and coarse particles, the choice of precursor is probably of no influence on the mechanism of particles precipitation[13]-[18].

Synthesis of submicrometer spherical alumina powders by spray pyrolysis is reported in this work. The influence of precursors ($Al(NO_3)_3 \cdot 9H_2O$ and $AlCl_3 \cdot 6H_2O$), and of process parameters on the formation mechanism of particles and their morphology have been studied. An equation for calculation of particle sizes produced by spray pyrolysis has been derived. The obtained results are in good agreement with the experimental data, and substantially better than the results obtained by Lang's equation[19].

II. Experimental Procedure

For the synthesis of alumina powders, 0.5 M water solutions of $AlCl_3 \cdot 6H_2O$ (for the A-1 powder) and $Al(NO_3)_3 \cdot 9H_2O$ (for the A-2 powder) were used as precursors.

A laboratory setup for the powder synthesis is shown in Fig. 1. It consists of an ultrasonic atomizer, a quartz tube reactor, and a system for powder collection. The atomization was done by means of an ultrasonic atomizer Gapusol-RBI-9001, with three transducers for aerosol generation from initial salt solutions, with a resonant frequency of 2.5 MHz and a capacity of 400 ml/h. It enables the formation of aerosol droplets with a mean particle size of 2 μm. The droplets were inserted into air stream (30 ~ 40 l/h) in the reactor at 1173 K. The residence time of droplets/particles inside the reactor was 95 s assuming the air flow rate and the droplets/particles velocity to be equal. The heating rate of droplets was 18 K/s. The particles were collected in a glass tube at the outlet of the reactor and in a bottle filled with distillated water.

Morphology and size of the particles, after spray pyrolysis and subsequent heating up to 1573 K was analyzed using micrographs obtained by a scanning electron microscope (SEM JEOL-JSM-5300), at a cathode voltage of 25 ~ 30 kV. The chemical composition was estimated by means of the energy dispersion analysis (EDS equipment Oxford Instruments QX-2000 S), in the range 0.5 ~ 20 keV. Thermal analysis (DTA and TGA) was done by means of a MOM Derivatograf C, up to 1573 K, at the heating rate of 0.25 K/s in air. The estimation of phase composition and transformations of powders after spray pyrolysis (after 2 h heating at 1073, 1173, 1273 and 1423 K) was done by a diffractometer Philips PW 1710, with CuKα radiation, in the range of angles of $2\theta = 5 \sim 60°$, and by an infrared (IR) spectrometer, Perkin Elmer 782, in the range of wave numbers from 400 cm^{-1} to 1600 cm^{-1}; the samples were prepared by the KBr method, with the ratio of the sample to KBr equal to 1:100.

III. Results and Discussion

1. Particle size distribution

The wave at the surface of liquid column induced by ultrasonic wave generator is shown in Fig. 2, where the coordinate of tangent line on the surface of liquid meniscus is marked as x, the perpendicular lines as y, the liquid density as ρ, the mean depth of the liquid column as h, the surface tension as σ, the liquid pressure near the surface of liquid column as p, and the amplitude of formed wave as $\xi(x, t)$. Now from Laplace's equation[20][21] the

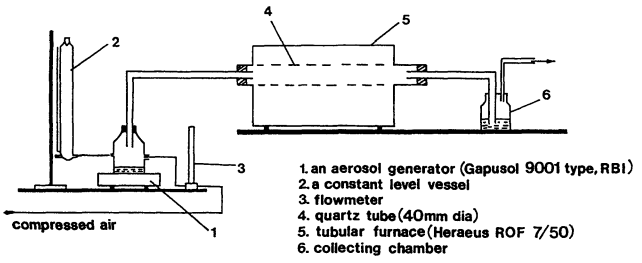

Fig. 1 Laboratory setup for the powder synthesis by ultrasonic spray pyrolysis.

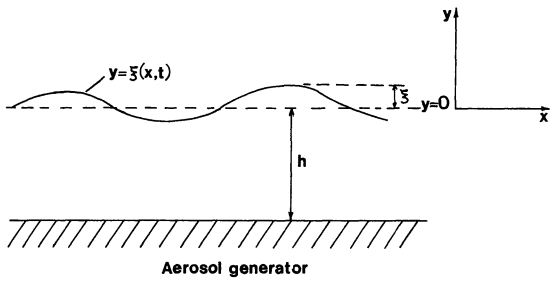

Fig. 2 The wave at the surface of liquid column induced by ultrasonic wave generator. (Symbols explained in the text.)

pressure is expressed by:

$$p=\sigma\left(\frac{\partial^2\xi}{dx^2}\right) \tag{1}$$

assuming that the internal pressure in the liquid, p, is much greater than the external pressure of the fluid outside the liquid.

If it is assumed that the liquid is incompressible, then from Bernoulli's equation[22] follows:

$$\rho gh+\frac{\rho d\varphi}{dt}+\sigma\left(\frac{\partial^2\xi}{dx^2}\right)=0 \tag{2}$$

where φ is the rate potential.

Since for boundary conditions $y=-h$, $v=0$, the condition $\nabla^2\varphi=0$ is satisfied, it follows that the rate potential is a harmonic function, which can be presented in the form

$$\varphi=\frac{1}{h}\frac{dy}{dt}ch[k(y+x)]e^{ikh} \tag{3}$$

where k is the wave number which can be expressed as $k=2\pi/d$, where d is the aerosol droplet diameter[21]-[23].

The relationship between the amplitude of oscillation of meniscus surface and the wave number, i.e. the wave length of the standing wave has a typical shape of Mathieu's function[23]:

$$\frac{d^2y}{dt^2}+\left[\frac{\sigma k^3}{\rho}th(kh)-kgth(kh)\right]y=0 \tag{4}$$

The solution of this differential equation, for sufficiently high h compared to that of the ultrasonic wave generated by the ultrasonic oscilator, is (same as in Ref. (24)):

$$d=\left(\frac{\pi\sigma}{\rho f^2}\right)^{1/3} \tag{5}$$

differing in numerical coefficients only from Lang's equation:

$$d_L=0.34\left(\frac{8\pi\sigma}{\rho f^2}\right)^{1/3} \tag{5a}$$

where f is the frequency of the ultrasonic wave.

For the calculation of the diameter of particles formed from aerosol droplets the following equation have been used[12]:

$$d_p=d\left(\frac{C_sM_o}{\rho M_s}\right)^{1/3} \tag{6}$$

where d_p is the diameter of particles formed from a droplet with diameter d, C_s is the concentration of initial solution (kg/m^3), M_o and M_s are molar masses of the produced oxide and the initial salt (kg/mol), respectively, and ρ is the oxide density (kg/m^3).

The particle diameters calculated from eqs. (5) and (6) are in better agreement with the experimentally determined mean particle diameters than with the values calculated from Lang's equation and eq. (6). Comparative values of the particle and droplet diameters obtained by various theoretical and experimental methods are shown in Table 1. For calculation of the droplet diameters in both cases, when eqs. (5) and (5a) has been applied respectively, the same values of the surface tension (72.9×10^{-3} N/m) and of the solution density (for Al-chloride and Al-nitrate, $\rho=1000$ kg/m^3) have been used.

Based on the statistical analysis of particle geometric parameters (Table 2 and Fig. 3), it is possible to conclude that beside the basic particle size given by the mean particle diameter, a wide spectrum of particle sizes has been registered with the Gauss/Maxwell Boltzman distribution curve. Such a distribution could be the result of degeneration of forced field frequency on the nuclei of elementary oscillators, i.e. droplets formed by the influence of spacial spheroidal complex waves, appearing owing to the superposition of all possible characteristic

Table 1 Calculated diameters of aerosol droplets and powders according to eqs. (5) and (5a) and experimentally determined particle diameters.

Powder	Aerosol droplet diameter calculated by eq. (5a) (μm)	Aerosol droplet diameter calculated by eq. (5) (μm)	Particle diameter calculated using droplet diameter according to eq. (5a) (μm)	Particle diameter calculated using droplet diameter according to eq. (5) (μm)	Experimentally obtained particle diameter (μm)
A_1	2.26	3.32	0.53	0.77	0.73
A_2	2.26	3.32	0.52	0.76	0.64

Table 2 Statistical analysis of geometric parameters of Al_2O_3 powders synthesized by spray pyrolysis.

Powder	Cross section area μm^2			Perimeter μm			Perimeter form factor			Area form factor			Diameter μm			Standard deviation
	min	max	mid	min	max	mid	min	max	mid	min	max	mid	min	max	mid	
A_1	0.02	3.21	0.49	0.51	6.96	2.37	0.64	1.03	0.95	0.94	1.02	0.99	0.17	2.08	0.73	0.19
A_2	0.05	1.37	0.35	0.79	4.33	2.07	0.67	0.99	0.96	0.96	1.03	1.00	0.22	1.31	0.64	0.25

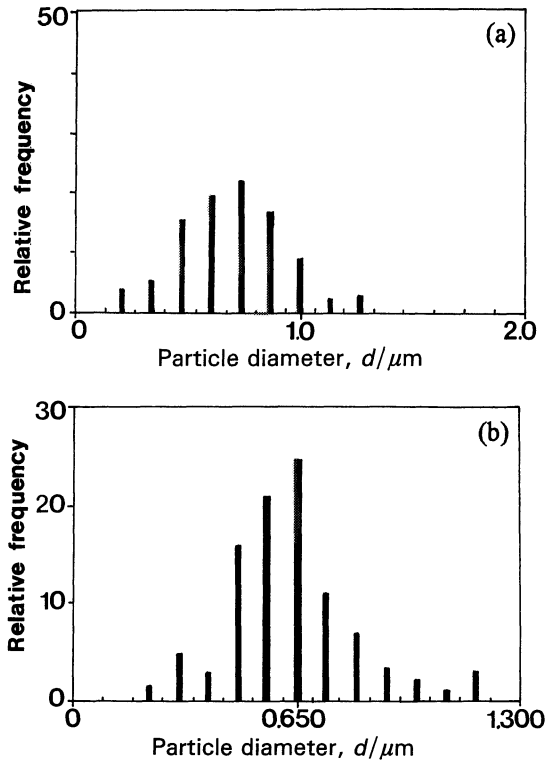

Fig. 3 Particle size distributions of Al_2O_3 powders produced by spray pyrolysis: (a) A-1 powder; (b) A-2 powder.

oscillations in the system. In a general case the complex wave, i.e. a package of waves is possible to describe by the Furie series, which could be, for any particular case, attributed to the spectrum of oscillations resulting in the registered geometric distribution of aerosol droplet diameters. Since the processes of coalescence and desintegration do not play a dominant role in particle solidification, the spectrum of particles correspond to the spectrum of droplets.

2. Particle morphology

Surface shape factors indicate that the produced particles are mostly spherical. Discrepancy in spheroidity of droplets generated inside the liquid continuum points to the ellipsoidal shape of waves, which at conditions of significant thickness of liquid film and surrounding viscosity have big curvatures. The separated droplet, as a highly elastic system tends to become spherical again outside the liquid. At the same time an interference of two types of oscillations occurs: oscillations caused by forced oscilator frequency, and oscillations caused by spontaneus tendency of the droplet to come back into the spherical shape under the action of surface tension. By the interference of these oscillations the "skin" effect may appear[25]-[27].

The particle morphology and the mechanism of precipitation inside the droplets have been determined indirectly by the SEM analysis.

Alumina powder, obtained by spray pyrolysis from

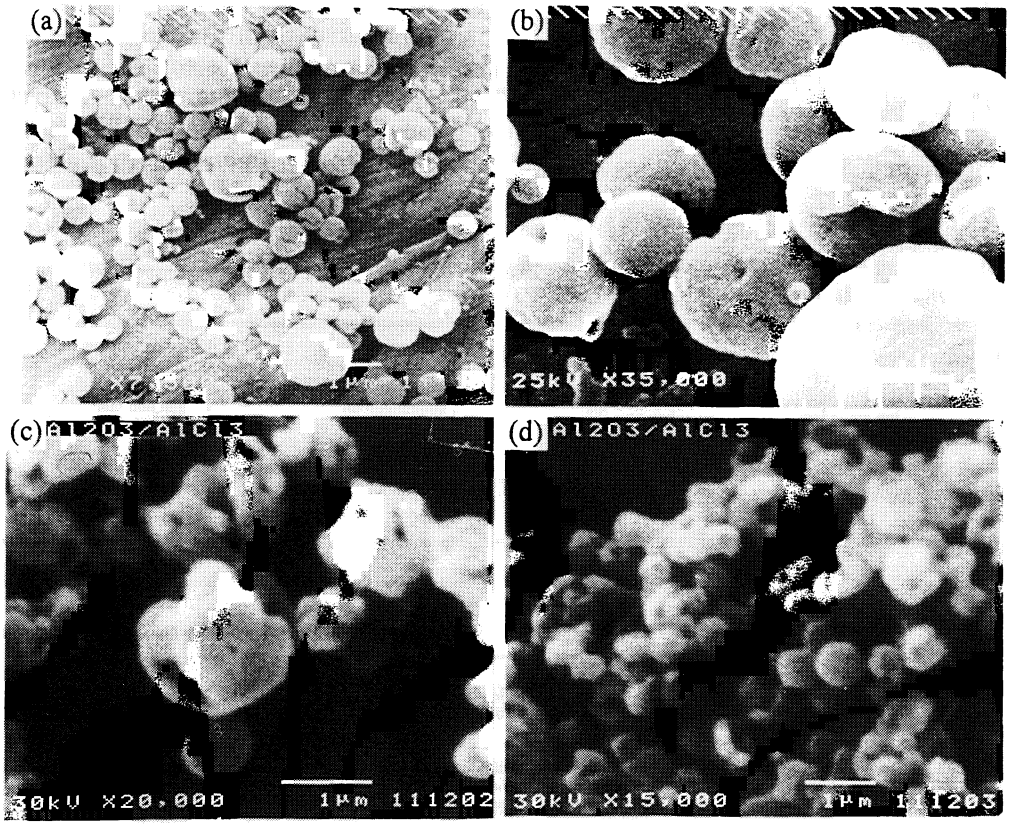

Fig. 4 SEM micrographs of the A-1 powder: (a) and (b) as sprayed; (c) and (d) after thermal treatment at 1573 K.

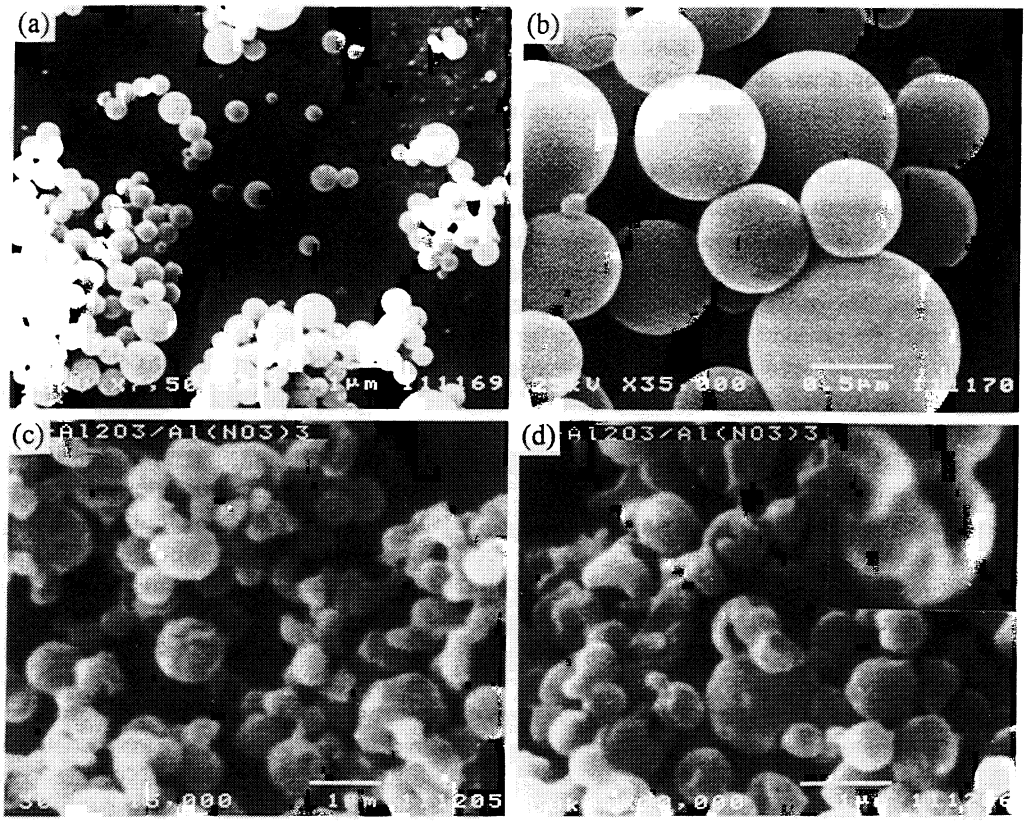

Fig. 5 SEM micrographs of the A-2 powder: (a) and (b) as sprayed; (c) and (d) after thermal treatment at 1573 K.

chlorides, shown in Fig. 4(a) and (b) is very fine with 80% of particle having sizes smaller than 0.5 μm. The spheres are mostly irregular with sponge-like structure, indicating their high porosity (nanometer pores) and high gas permeability. This morphology could be a result of $AlCl_3$ evaporation from the particle surface. Beside them, fine satellite spheres formed by the fragmentation of larger spheres (up to 100 nm) and coarser spheres (up to 2 μm) have also been detected (5 ~ 10% of overall spheres total quantity). As can be seen from Fig. 4(c) and (d), the spheres are polygonal (with sexangular curvature) after the calcination process. A great number of spheres have been sintered, and well developed contact necks on the grain boundaries (particle contacts) are observed. Due to an additional shrinkage during sintering, more than a half of all spheres have diameters up to 300 nm. Spheres larger than 1 μm are cracked in polar area forming characteristic curvatures (cavities)[27]. The substructure (secondary structure) is obvious. It consists of particles of different sizes and "free volumes" between the particles. In the case of particles of 0.5 ~ 1 μm, welded fragments and cracking lines formed in the process of subsequent desintegration, are also present. Knot points connecting structure fragments and free volumes inside the particle can be connected with the intensity of interaction between substructure particles. In some areas chipped fragments or enlarged particle deformations are evident as the result of densification inside the particle during sintering and denser central bonding of fragments, leading to the emphasised oscillation transport of knot points on the particle surface during both the precipitation and the solidification. The internal structure on the particle level is complex, and consists of a series of particles and missing fragments.

Alumina particles obtained from nitrates by the spray pyrolysis are shown in Fig. 5(a) and (b). They are highly spheroidal and ideally smooth with uniform diameters smaller than 0.5 μm (80%). About 10% of particles is smaller than 300 nm and 5 ~ 10% is near to 1 μm (a few of them are near to 2 μm). Missing fragments at larger particles can be found at the pole-directions of the central axis, that links the fragments of substructures and "free volumes". Figures 5(c) and (d) (after calcination at 1573 K) show the particles with polyhedral surfaces, and a significant number of twin particles. Cracked particles of a shell-like structure (as dominant) indicate a concentration of a number of free volumes in the particle centre. Particles smaller than 400 nm have minute cavities, but fine particles (smaller than 100 nm) are without them. The particle appearance points out the large concentration gradient of salt melt (the melting point of 349 K), that precipitates through the droplet surface. This gradient is a result of a difference between the rates of solvent evaporation inside the droplet/particle and on its surface. The high packing density on the particle surface, the particle smoothness, and the particle surface rigidity cause the low permeability and the fracture along boundaries of particle substructure because of high vapour

pressures conserved in the particle. Inside the particle elongated cylinders are registered, displaying that the particle is consisted of a number of spherical subparticles, whose floculation and/or coalescence occur along a preferred direction[27].

Many parameters, in both cases, effect the particle morphology. Their influence depends on both physico-chemical characteristics of the given system and on the size of aerosol droplets exposed to the precipitation and solidification processes. The most significant factors are:

—morphology and the physical field responsable for the droplet excitation[27] (droplet excitation has been considered as specially important process for droplet formation and particle history, which by the precipitation under the influence of a high temperature field results in the final morphology of the particle),

—temperature gradient between the surface and the centre of droplet/particle,

—thermal surface waves and the type of changes in the system being a consequence of superposition of these waves with those coused by the droplet excitation field during the droplet genesis,

—viscoelastic properties of the droplet (character and level of its rigidity, and droplet behaviour during its collision with other aerosol droplets)[27],

—coalescence[12],

—thermodiffusion coefficient,

—permeability of the shell formed on droplet surface during its solidification.

In the case of fine particles (smaller than 0.3 μm), the most important particle morphology factor is the excitation field which generates the aerosol droplets.

The other important parameter, which determines the mode of particle precipitation and its morphology, is time, t_{eq}, at which the temperature in the bulk of the droplet becomes equal to the surface temperature. If this time is short enough, an uniform supersaturation of the solution in the bulk of droplet (the volume precipitation) will occur.

Furier's equation for the heat conduction[28] can be expressed in the following form:

$$\chi \Delta T_n = -\lambda T_n \tag{7}$$

where χ is the coefficient of temperature conductivity, T_n is the orthogonal radial function of temperature, and $\lambda = 1/t_{eq}$. Using eq. (7) it is possible to estimate the time of temperature equalizing in the bulk of the droplet.

Owing to the isotropic medium, centrally symmetric solution of eq. (7) can be expressed as:

$$T_n = T_0 \cos\left(\frac{\pi r}{R}\right) \tag{8}$$

where T_0 is the temperature of the droplet surface, r is perpendicular distance between the temperature wave front and the surface of the droplet, and R is radius of the droplet.

The temperature coefficient of conductivity can be expressed as

$$\chi = \frac{k}{\rho c_p} \tag{9}$$

where k is the coefficient of heat conductivity, ρ is the density of the droplet, and c_p is the specific heat at constant pressure. It follows that the time of temperature equalization at the surface and in the bulk of the droplet, t_{eq}, can be written as:

$$t_{eq} = \frac{d^2}{\chi \pi^2} \tag{10}$$

where d is the diameter of the droplet.

Since the time needed for diffusion in the liquid phase $t_{eqD}(t_{eqD} = d^2/D\pi$ where D is the diffusion coefficient of dissolved substance[12][28]) is much shorter than t_{eq}, it follows that in the case of a droplet, sufficiently small in diameter, during t_{eq} no significant changes in the solution concentration in the bulk of droplet occur. It is the reason of homogeneous saturation of the solution of aerosol droplet and its volume precipitation. If the mentioned condition is not fulfilled, as in the case of large aerosol droplets, the mechanism of precipitation and the droplet destruction will be tightly connected with other characteristics of the system, e.g. the coefficient of temperature solubility of precursors, difference between the critical supersaturation of solution and the equilibrium saturation, thermoplastic properties of the salt melt, etc.

The formation mechanism of the hollow spheres by continuous evaporation of solvent from the droplet bulk, resulting in an increase in melt viscosity, is mostly concerned with larger droplets[12] whose solidified surfaces become closed when critical supersaturation is reached. If the salt melting occurs when the particles are exposed to the high temperature field, then a non-permeable shell is formed. It inhibits the processes of relaxation of internal thermal stresses appearing during the evaporation of solvent remained in droplet bulk. Hence, in the case of particles obtained from Al-nitrate solution, particle cracking occurs. Cracking is more pronounced here than in the case of Al-chloride used as a precursor.

It follows directly from Fourier's equation that there is some critical time and critical rate of temperature equalizing in the whole droplet. The precursor properties are not, therefore, of dominant importance for development of the particle morphology and for the microstructure formation inside the particle.

3. Phase analysis

It can be seen from the EDS analysis of the powder A-1, shown in Fig. 6(a), that the decomposition of Al-chloride has not been completed. Similar thing has happend with the powder A-2, obtained from Al-nitrate, although it is not directly obvious from Fig. 6(b), because the method is not sensitive enough to register the nitrogen atoms.

It is also evident from DTA and TGA, shown in Fig. 7(a) and (b), that the decomposition of the amorphous powders A-1 and A-2 has not been completed. Decomposition of the initial and formed compounds in the A-1

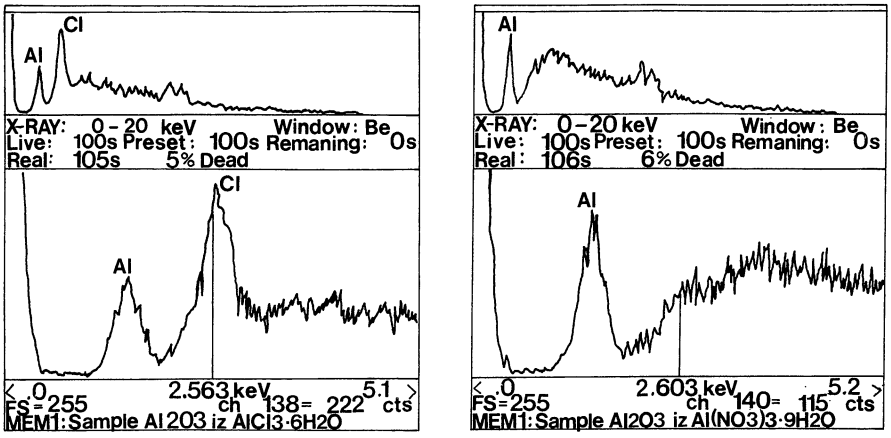

Fig. 6 EDS analysis of Al_2O_3 powders obtained by ultrasonic spray pyrolysis: (a) A-1 powder; (b) A-2 powder.

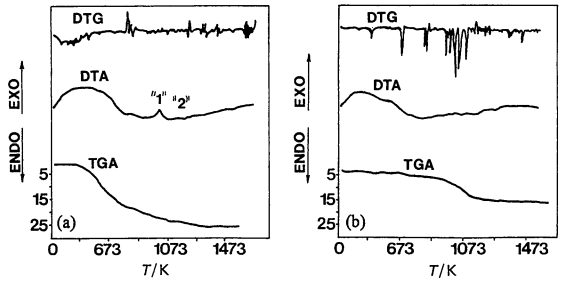

Fig. 7 DTA and TGA data for Al_2O_3 powders: (a) A-1 powder; (b) A-2 powder

and A-2 powders is intensive up to 953 and 1053 K, respectively. Decomposition of the A-1 powder, according to TGA, is possible up to 1373 K. At such a high temperature, decomposition of the remained chlorides and eventually the evaporation of OH-groups and chlorine from γ-Al_2O_3 proceed[8]. The weight loss between 973 and 1073 K is also determined from TGA, which could be connected with the evaporation of remained nitrates and OH-groups from γ-Al_2O_3. DTA of the A-1 powder (Fig. 7(a)) shows the first exothermal peak "1" at around 1053 K, which could be a result of the γ-Al_2O_3 crystallization from the amorphous phase, and the second exothermal peak "2" at approximately 1153 K, corresponding probably to the phase transformation of γ-Al_2O_3 to α-Al_2O_3. DTA of the A-2 powder (Fig. 7(b)) shows a series of consecutive peaks of low intensity, which cannot be clearly identified.

X-ray analysis of the initial powder obtained by spray pyrolysis at 1173 K (Fig. 8(a) and (b)) shows that the A-1 and A-2 powders are amorphous, indicating that the residence time and temperature of the solidified droplets are not sufficient for occurence of the crystallization.

X-ray analysis of the A-1 powder (Fig. 8(a)) shows, in the case of the sample heated at 1073 K, the diffraction peaks corresponding to γ-Al_2O_3. Diffractogram of the same sample heated at 1173 K corresponds to the presence of both γ- and α-alumina. Diffractograms of samples heated at 1273 and 1423 K show the presence of

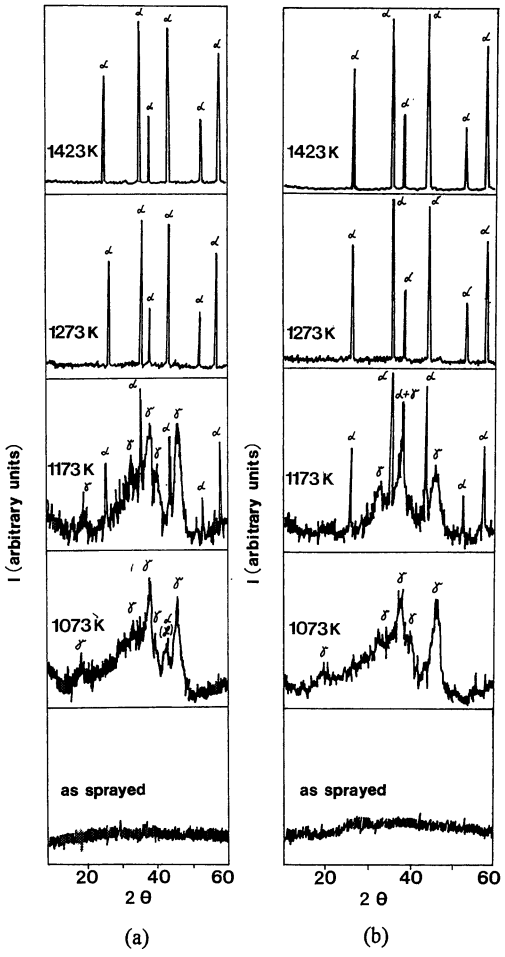

Fig. 8 Diffractograms of Al_2O_3 powders: (a) A-1; (b) A-2, obtained by ultrasonic spray pyrolysis and subsequently heated at different temperatures.

the well crystallized α-phase only. In the case of the sample heated at 1423 K the peaks are more intensive.

X-ray analysis of the A-2 powder (Fig. 8(b)) shows the diffraction peaks characteristic for γ-alumina in the case of the sample heated at 1073 K. Diffractogram of the sample heated at 1173 K confirms the presence of both α- and

γ-alumina. The peaks corresponding to the α-phase in the A-2 powder are more intensive than in the case of A-1 powder heated at the same temperature. It means that the transformation process of γ- into α-Al_2O_3 is faster in the case of nitrate ions than in the case of chloride ions. Diffractograms of the same sample heated at 1273 and 1423 K show the presence of well crystallized α-alumina, but the peaks are more intensive for the A-2 sample. It means again that the transformation into α-alumina is faster in the case of the A-2 samples.

There is a significant difference between the obtained results and the data from references[29][30] (according to them the phase transformation of γ- into α-alumina occurs in the range 1323 ~ 1373 K). It means that the powders produced by the spray pyrolysis are very active, and that in the transformation process the presence of Cl^-, NO_3^- and OH^- ions, already in the amorphous structure of powders, plays an important role. The crystallization of γ-alumina from the amorphous phase between 773 and 873 K is facilitated by the presence of remained Cl^-, NO_3^- and OH^- ions which stabilize its structure. Evaporation of chlorides, OH^- ions, and nitrogen oxides from the structure of γ-alumina occurs in the temperature range 1073 ~ 1173 K, accelerating the process of transformation of transient phases into α-alumina. The parameters important for that phase transformation are: the ion sizes, the electric charges, the concentration, and the ion distributions. Since the last three parameters are the same for both powders, it is obvious that the ion sizes have a dominant influence on the rate of phase transformation.

IR spectrum of the A-1 powder (Fig. 9(a)) heated at 1073 K, is characteristic for γ-alumina[31][32]. It contains the broad absorption bands in the ranges 550 ~ 600 cm^{-1} and 700 ~ 780 cm^{-1}. In the case of the sample heated at 1173 K, the beginning of absorption band at 480 cm^{-1} and its intensification at 590 cm^{-1} indicate that the crystallization of α-alumina has occurred. For the samples heated at 1273 and 1423 K, the bands characteristic for α-alumina only have been registered and their intensity is prominent in the case of sample heated at higher temperature.

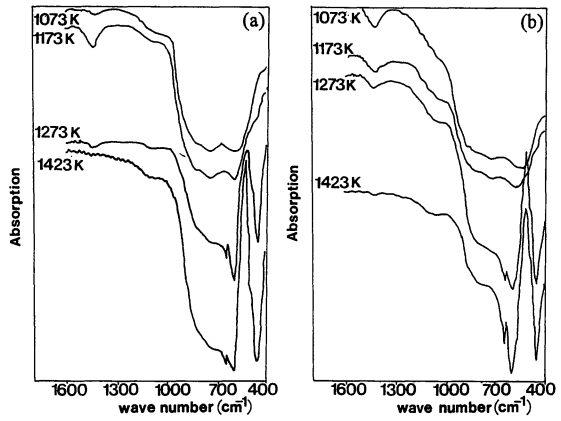

Fig. 9 IR analysis of Al_2O_3 powders: (a) A-1; (b) A-2, obtained by ultrasonic spray pyrolysis and subsequently heated at different temperatures.

IR spectrum of the A-2 powder heated at 1073 K (Fig. 9(b)) has the absorption bands characteristic for γ-alumina. Their intensity is lower than the intensity of the same bands of the A-1 sample, indicating higher degree of crystallization in the crystal lattice of the A-1 sample, which contains smaller in size Cl^- ions compared to NO_3^- ions in the A-2 sample. At 1173 K, the band at 590 cm^{-1} is shifted and more intensive, and a new band appears at 480 cm^{-1}. Samples heated at 1273 and 1423 K have the absorption bands characteristic for α-alumina. Higher intensity of the bands at elevated temperature is the consequence of higher degree of crystallinity and better order of the system.

IV. Conclusion

The formation mechanism of aerosol droplets obtained by ultrasonic spray pyrolysis have been discussed. Phenomenological analysis of a droplet genesis shows the manner of droplet formation. The particle sizes (calculated using eq. (5) derived on the assumption that the aerosol droplet represents a mechanical oscillator excited by the complex ellipsoido-spherical wave inside the reactor) were compared with the results obtained using Lang's equation.

The particle size distribution was analyzed considering the degeneration of forced frequency of ultrasonic oscillator.

The morphology of particles and the mode of their precipitation were analyzed from the standpoint of the rate of reaching temperature equilibrium inside the droplets. For both powders, A-1 and A-2, it is shown that the mechanism of precipitation, according to Furier's equations, is dominantly dependent on the diameter of aerosol droplet. For the droplet diameters smaller than 1.3 μm (the particle diameters smaller than 300 nm), the mechanism of volume precipitation is dominant because of extremely short time of temperature equalizing between the centre and the surface of droplet. It provides conditions for equilibrium supersaturation of the solution in the bulk of droplet in a short time, and for the precipitation along the whole diameter. Further, for larger droplet diameters (diameters larger than 4 μm, and the coresponding particles larger than 1 μm) the mechanism of surface precipitation is dominant. In this case, the influence of precursor on the mode of precipitation inside the aerosol droplet is important as well as other parameters: temperature coefficient of solubility, difference between critical supersaturation and equilibrium saturation of the solution, permeability of the solid shell formed firstly at the surface, precursor melting before the complete solidification, etc.

The powders obtained by ultrasonic spray pyrolysis of aerosol have a high spheroidity, e.g. the A-2 powder, prepared from Al-nitrate solution has the factor of spheroidity equal to 1.0. The mean particle size of the produced powders is 0.730 μm and 0.640 μm for the A-1 and A-2 powders, respectively.

Based on DTA, TGA, IR, and X-ray analysis of the A-1 powder heated at 1073, 1173, 1273, and 1423 K for 2 hours, it is concluded that in both powders A-1 and A-2 the crystallization of γ-alumina from the amorphous phase occurs at temperatures below 1073 K, and the phase transformation of γ- into α-alumina occurs between 1073 and 1173 K. At 1273 K, α-alumina only is present. In the case of the samples heated at 1423 K higher degree of crystallinity is registered. From the diffraction peak intensities and adsorption IR spectra, it is obvious that the degree of crystallinity is higher in the case of the A-2 powder, produced from nitrate solution, compared to the A-1 powder, produced from chloride solution, because the bigger nitrate ions destabilize the structure of γ-alumina to a greater extent at higher temperatures compared to the chloride ions present in the A-1 powder.

Acknowledgement

This research was financially supported by the Republic Ministry of Sciences and Technology. The authors gratefully acknowledge Drs. Lj. Živković, B. Jordović, Ž. Živković, Lj. Karanović and R. Petronijević for SEM, EDS, statistical, DT/TG, X-Ray and IR analysis.

REFERENCES

(1) M. Formeti, F. Juillet, P. Meriandeau, S. J. Teichner, P. Vergnon: J. Colloid and Interface Sci., **39** (1972), 79.
(2) B. W. Johnson: Am. Ceram. Soc. Bull., **60** (1981), 221.
(3) J. P. Bach, F. Thenvenat: J. Mat. Sci., **24** (1989), 2711.
(4) F. Juillet, F. Lecomte, H. Mozzanega, S. J. Teichner, A. Therent, P. Vergnon: Faraday Symposya of the Chemical Society, N7 (1973), 57.
(5) W. F. Kladnig and W. Karner: Ceram. Bull., **69** (1990), 814.
(6) R. S. Ehle, B. J. Baligna, W. Katz: J. Electron. Mater., **12** (1983), 587.
(7) D. P. Stinon, T. M. Besmann, R. A. Lowden: Am. Ceram. Soc. Bull., **67** (1988), 350.
(8) M. J. Ruthner and H. Krischner: *I.C.S.O.B.A. 3e Congress International*, Nice, France, (1973), p. 547.
(9) T. Haug, M. Fandel and T. Staneff: Powd. Metal. Int., **22** (1990), 32.
(10) D. M. Roy, R. R. Neurgaonkar, T. P. O'Holleran and R. Roy: Ceram. Bull., **56** (1977), 1023.
(11) S. C. Zhang and G. L. Messing: *Ceramic Transaction, vol. 12, Ceramic Powder Science III*, Ed. by G. L. Messing, S. Hirano and H. Hausner, American Ceramic Society, Westerwille, OH, (1990), p. 49.
(12) G. L. Messing, S. C. Zhang and G. V. Jayanthi: J. Am. Ceram. Soc., **76** (1993), 2707.
(13) Y. Kanno and T. Suzuki: J. Mater. Sci., **23** (1988), 3067.
(14) H. Anderson, T. T. Kodas and D. M. Smith: Ceram. Bull., **68** (1989), 996.
(15) O. Milošević, B. Jordović and D. Uskoković: Mater. Lett., **19** (1994), 165.
(16) O. Milošević and D. Uskoković: Mater. Sci. Eng., **A168** (1993), 249.
(17) S. Stopić, I. Ilić, D. Uskoković: Mat. Lett., **24** (1995), 369.
(18) Dj. Janaćković, V. Jokanović, Lj. Živković, Lj. Kostić-Gvozdenović and D. Uskoković: *Proceedings of World Ceramic Congress-Eight Cimtec, Ceramics: Charting the Future, Advances in Science and Technology*, Ed. by P. Vincenzini, Techna, Faenca, (1995), p. 1229.
(19) R. J. Lang: J. Acoust. Soc. Am., **34** (1962), 6.
(20) K. F. Herzfeld, T. A. Litovitz: *Absorption and Dispersion of Ultrasonic Waves*, Academic Press, New York, London, (1959).
(21) L. D. Landau, E. M. Lifšic: *Mehanika Neprekidnie Sredi*, AN SSSR, Moskva, (1960).
(22) V. G. Levič: *Fizikohimijčeskaya hidrodinamika*, AN SSSR, Moskva, (1952).
(23) N. W. Mc Lachlan: *Theory and Applications of Matheiu Functions*, Oxford University Press, London, (1947).
(24) R. L. Peskin and R. J. Raco: J. Acoust. Soc. Am., **35** (1963), 1378.
(25) A. M. Spasić, V. Jokanović and D. Krstić: "Physical Nature of the Structure of Electrified Liquid-Liquid Interfaces", 187th Meeting of the American Electrochemical Society, Reno, (1995).
(26) A. M. Spasić and V. Jokanović: *The Secondary Liquid-Liquid Electro-Mechanical Oscilator*, CHISA, Prague, (1993).
(27) A. M. Spasić and V. Jokanović: J. Colloid Interface Sci., **170** (1995), 229.
(28) F. Kamenecki: *Difuzii i Perenos Teploty v Himičeskoi Kinetike*, AN SSSR, Moskva, (1947).
(29) N. M. Drobot, K. G. Ione and N. E. Bujanova: Kinetika i Kataliz, **6** (1970), 1537.
(30) A. M. Kalinina and E. A. Porai-Kosic: Doklad Akademii Nauk SSSR, **2** (1957), 365.
(31) K. Okada and N. Otsuka: J. Am. Ceram. Soc., **69** (1986), 652.
(32) M. Ocana, V. Fornes and C. J. Serna: Ceram. Int., **18** (1992), 99.